crystals

MDPI

Article

Effect of Diazotated Sulphonated Polystyrene Films on the Calcium Oxalate Crystallization

Patricio Vásquez-Quitral [1], Javier Toledo Arana [2], Maria Cristina Miras [2], Diego Fernando Acevedo [2], Cesar Alfredo Barbero [2] and Andrónico Neira-Carrillo [1,*]

[1] Department of Biological and Animal Sciences, School of Veterinary and Animal Sciences, University of Chile, Santiago, P.O. Box 2-15, Chile; pvasquitral@yahoo.com

[2] School of Sciences Exact, Physico-Chemical and Natural, National University of Rio Cuarto, Rio Cuarto, Cordoba, P.O. Box X5804BYA, Argentina; jtoledoarana@gmail.com (J.T.A.); mmiras@exa.unrc.edu.ar (M.C.M.); dacevedofernando@gmail.com (D.F.A.); cbarbero@exa.unrc.edu.ar (C.A.B.)

* Correspondence: aneira@uchile.cl; Tel.: +56-22-9785642

Academic Editor: Gianluca Di Profio

Received: 1 August 2016; Accepted: 25 February 2017; Published: 28 February 2017

Abstract: Pathological crystallization of calcium oxalate (CaOx) inside the urinary tract is called calculi or kidney stone (Urolithiasis). CaOx exhibits three crystalline types in nature: CaOx monohydrate COM, dihydrate COD and trihydrate COT. COD and COM are often found in urinary calculi, particularly COM. Langmuir monolayers, membrane vesicles, phospholipids' micelles, among others, have been adopted as simplified biomimetic template-models to study in vitro the urolithiasis through CaOx. The nucleation and crystal growth of COM on self-assembled lipid monolayers have revealed that the negatively charged phosphatidylserine interface is a strong promoter of COM. Herein, we describe the synthesis and physicochemical characterization of diazotated sulphonated polystyrene films (DSPFs), prepared from various aminocompounds varying their polarity degree i.e., polar, non-polar and acidic DSPF derivatives. We also used these DSPFs as polymeric templates in crystallization experiments of CaOx in vitro. Images obtained by optical microscopy and scanning electron microscopy confirmed the precipitation of COM crystals on the DSPF surface. The employment of functionalized polymeric films as templates for CaOx crystallization represents a viable approach for understanding inorganic mineralization.

Keywords: crystallization; calcium oxalate; polystyrene films; sulphonation; diazotation

1. Introduction

Urolithiasis is defined as a pathological formation of polycrystalline aggregates or human kidney stones (HKS) inside the urinary tract. This process involves four steps: nucleation, growth, aggregation and retention of crystals [1]. HKS can be constituted by one or more inorganic components such as calcium oxalate, cystine, calcium phosphate, struvite and uric acid. CaOx is one of the most abundant biominerals in superior plants [2] and represents the most abundant inorganic compound found in mammal urinary calculi [3]. CaOx exhibits three crystalline types in nature: CaOx monohydrate COM, CaOx dihydrate COD, and trihydrate COT. COM is the most stable thermodynamically and it is frequently found in HKS. Numerous factors have been stated as direct or indirect causes of the formation of HKS: mechanistic and/or kinetic [4], dietary [5,6], genetic [7–9], climatic [10], among others. It has been demonstrated that both, organic and inorganic substances, exhibit a modulating effect on CaOx crystallization [11]. Urine volume inferior to 2–3 L/day [12], urinary pH less than 5.8 [13], concentrations of calcium ions (Ca^{2+}) in urine superior to 0.1 mmol/Kg/24 h [14] and of oxalate (Ox^{2-}) superior to 40 mg/24 h [15] are known to promote the formation of HKS. Specifically, the excess of Ox^{2-} in the urine of these patients may deposit on the membrane of renal

tubular epithelium cells, triggering necrosis and/or apoptosis. In vitro studies revealed that renal proximal tubular brush-border membranes are involved in the CaOx crystallization, suggesting that urinary macromolecules such as lipids play a critical role in urolithiasis [16]. Alteration of composition, structure and/or concentration of some important urinary molecules, either free in urine or forming part of the cell's membrane, is going to promote the formation of COM. Langmuir monolayers [17,18], bilayers, membrane vesicles [19], phospholipids, micelles [20], self-assembled monolayers (SAMs) [21], etc., have been used as biomimetic models to study the in vitro crystallization of CaOx. For instance, reports of COM crystals' nucleation and growth on SAMs revealed that a negatively charged phosphatidylserine (PS) interface is a strong promoter of COM [22]. Moreover, the effects of dipalmitoylphosphatidylcholine (DPPC) monolayers on the CaOx mineralization, from solutions containing chondroitin sulfate have been reported [23]. Chondroitin sulfate A (C4S) and C (C6S) correspond to polyanionic polysaccharides that act as macromolecular inhibitors of the pathological mineralization of CaOx [24–27]. On the other hand, COM grown under DPPC monolayers were three-dimensional hexagonal prisms and well separated with a mean size of 8 μm × 5 μm × 4 μm. COM grown under DPPC monolayers in the presence of C6S were strongly elongated hexagonal plates due to the inhibition of lateral growth. C6S is adsorbed at the face (1 0 1) of COM, therefore further growth at this face is inhibited. The (1 0 1) face of the COM is characterized by Ox^{2-} that emerge oblique to the surface face with a dense pattern of complexed Ca^{2+} [27–29]. After one Ox^{2-} layer is complexed with Ca^{2+}, the face (1 0 1) will become rich in calcium with a positively charged surface. The headgroups of DPCC monolayers are zwitterionic phosphatidylcholine (PC), thus it is not appropriate to consider only the electrostatic attraction between DPCC and Ca^{2+}. There is some attractive interaction between the headgroup of PC and Ca^{2+}, which may lead to the growth block of the face (1 0 1), but stabilizing it at the same time. In contrast, the face (0 2 0) of COM is nearly neutral, containing an alternative arrangement of Ca^{2+} and Ox^{2-}. The Ox^{2-} lie on the surface crystal COM with a perpendicular orientation to the face (0 2 0) [27]. Therefore, it could be less favorable for DPCC headgroups' interaction with the face (0 2 0). Ca^{2+} can generate the sulfate salt of C6S, and interact with other polar groups in the C6S backbone [4]. Thus, it is rational to believe that under DPPC monolayers, and in the presence of the C6S face (1 0 1), there is simultaneous interaction with C6S and the negatively charged phosphate headgroups of the DPPC monolayer. The stabilization of the face (1 0 1) could be further enhanced by increasing the concentration of C6S, and the preferential growth along the b-axis could also be induced. He and Ouyang (2009) used DPCC Langmuir–Blodgett (LB) films to study the nucleation and growth of CaOx crystals in vitro [30,31]. In turn, the interface tension line promotes the formation of circular discrete domains (CDDs) [32,33]. SEM showed that the diameter of these CaOx crystal patterns ranged from 10 to 200 μm. CaOx was often located at the boundaries of both the larger domains and the small domains in large LC domains, building up round-shaped growth regions of crystals. Specifically, nucleation was attributed to the monolayer structure relaxation and the reorganization of amphipathic molecules, which matched with the nucleating crystal face. The formation of the defective LC domains in the LB films was attributed to the molecular arrays in LB films, especially at the boundaries that were destroyed by $K_2C_2O_4$ due to the interaction between the negatively charged Ox^{2-} and the phosphatidic groups of DPPC headgroups [17,34,35]. Although the boundaries can be introduced into LF films through the transfer process onto the solid support [36–38], the DPCC LB films without $K_2C_2O_4$ solution cannot induce formation of circular patterns of COM crystal. In this case, scarce crystals COM hexagonal elongated of 5–10 μm length were formed at the boundaries of DPPC LB films. XRD confirmed the existence of the plane (0 2 0), previously mentioned for COM. These results would shed light on the relationship between the injury of renal epithelial membrane and urolithiasis. Moreover, An et al. (2010) fabricated patterns of phosphatidylserine (DPPS) bilayers and osteopontin (OPN) on silica substrates to create spatially organized surfaces of macromolecules [39]. These patterns allowed the renal tubule surface to be mimicked, and the adhesion of COM crystals to regions with different biochemical composition to be evaluated. Subsequent exposure of the OPN-patterned surface to unilamellar vesicles comprising

DPPS and 2 mol % 1,2-dioleoyl-sn-glycero-3-phosphoethanolamine-*N*-carboxyfluorescein (DOPE-CF) generated a lipid bilayer membrane in corrals surrounded by the existing OPN grids through fusion onto the bare regions of the substrate. The fidelity of the DPPS–OPN patterns was confirmed by epifluorescence analysis, which revealed the carboxyfluorescein chromophore (green) in the lipid regions, and the Texas Red chromophore (red) in the OPN regions. Micrometer-sized COM dispersed in 1 mM CaOx solutions attached preferentially to the OPN regions, in agreement with other studies performed in vitro that have suggested a binding affinity of OPN to COM crystal surfaces [40]. COM collected from fresh CaOx solutions (2 min) measured ~3 μm in length, suggesting that the crystals observed on the OPN regions attached as mature crystals, migrating to these regions through Brownian motion [41] rather than growing from nuclei that had formed preferentially on OPN. The attached microcrystals increased in size at longer immersion times, which was consistent with the sizes of crystals harvested from the solution at periodic intervals. These COM grew to nearly 6 μm after 60 min, and 10–20 μm after 24 h. In addition, OPN adsorbs on the COM surface, suppressing the attachment of these crystals to DPSS; suggesting a remarkable association between OPN and reduced attachment of COM crystals to renal epithelium [42]. An et al. (2010) point out that this patterning protocol can be expanded to other urinary molecules, providing a convenient approach for understanding the effects of biomolecules on the attachment of COM crystals, and the pathogenesis of kidney stones. Previously, we were able to selectively control the morphology of CaOx by using the electrochemical technique [43]. More recently, we evaluated the effect of multiwalled carbon nanotubes (MWCNT) oxidized and functionalized with different chemical compounds carrying acidic groups (–COOH) on CaOx crystallization. Although naturally occurring urinary micro and macromolecules [1,3,11,44] are believed to play an important role in controlling the HKS formation, a mechanistic understanding is still missing. Herein, we describe the synthesis and characterization of diazotated sulphonated polystyrene films (DSPF), and their utilization as polymeric templates for selective in vitro CaOx crystallization.

2. Results and Discussion

Sulfonic functional groups have been reported to be introduced to polymer surfaces by solution-based sulfonation reactions in work led by Leonor [45]. High molecular weight (HMW) polyethylene (HMWPE) plates were sulfonated by a heterogeneous reaction involving treatment with 50 vol % chlorosulfonic acid [46–49]. For the functionalization of polyethylene terephthalate (PET), Nylon-6 and the ethylene vinylalcohol (EVOH), they applied a sulfuric acid solution at concentrations from 10 to 50 vol % depending on the substrate [45,46]. They reported successful introduction of the sulfonic group based on Fourier transform infrared spectroscopy (FTIR) and no evidence of degradation of the bulk polymers was determined. On the other hand, Suzuki et al. synthesized phosphate-containing homo- and block-copolymers by reversible addition fragmentation chain transfer [RAFT] using mono(2-acryloyloxyethyl) phosphate (MAEP) and 2-(metha-cryloyloxy) ethyl phosphate (MOEP), phosphate-containing monomers, together with the monomer acetoacetoxy-ethyl-methacrylate (AAEMA) [50,51]. Due to the large amount of diene in these monomers, the resulting polymers were highly branched when keeping the low MW of polymers and resulted in a gel when higher MWs were attempted. Films were produced either by direct casting of the homo-polymers [50], by adsorbing polyacetoacetoxy-ethyl-methacrylate (PMOEP) homopolymer to a poly(ethylene diamine) modified surface [51], or by attaching the block-copolymer to an aminated surface [50,51]. A different approached to the synthesis of phosphate-containing polymers was presented by Stancu et al. who made random copolymers using the monomer MOEP and either diethylamino ethyl methacrylate (DEAEMA) or 1-vinyl-2-pyrrolidinone (VP) [52]. In the (PMOEP-*co*-DEAEMA) copolymers, the monomer units were found to be distributed homogenously, unlike the (PMOEP-*co*-VP) copolymers, where the MOEP was consumed before total conversion and was achieved resulting in short VP segments [52]. Ethirajan et al. produced nanoparticulate copolymers of styrene and acrylic acid (AAc) using a mini-emulsion copolymerization reaction with

ionic and non-ionic surfactants. Through titration, it was demonstrated that the concentration of surface carboxylate groups increased with increasing AAc content. In addition, it was found that a higher surface charge density of the functional groups could be achieved with the use of the non-ionic surfactant [53]. Moreover, Miyazaki et al. produced aromatic polyamide copolymers with 0, 20 and 50 mol % of the monomer units containing carboxyl groups. Films were produced either without or with calcium chloride added to the casting solution [54]. By the same method, Kawai et al. prepared aromatic polyamide copolymers with a similar stoichiometric monomer ratio containing sulfonic groups ($–SO_3H$) and using films produced with and without $CaCl_2$ [55].

In our work, functionalization was carried out so that the surface of polystyrene (PS) films' possesses spatial charge distribution of different functional groups, hence different physicochemical properties, and thus changes form to crystallize CaOx; this is similar to what occurs with biological molecules in biogenic mineralization such as bone and $CaCO_3$ mineralization. PS films were sulphonated through a surface chemical reaction, which gave them anionic moieties groups of sulfonic groups ($–SO_3H$). PS films were submerged in a 10% solution of fuming sulfuric acid containing 65% of SO_3 and 90% of concentrated sulfuric acid during 30 min. Then, these sulfonated polystyrene (PSS) films were surface-chemically modified by using diazonium salts with the following amine compounds: aniline, 2-chloroaniline, 4-hexadecylaniline, 4-dodecylaniline, o-anisidine and 6-chloro-2,4-dinitroaniline (Please see Suplementary Material, Figure S1). Scheme 1 shows the reaction between the polymeric films and the diazonium salts through several amino-synthesized compounds. As shown in Figure 1, the result was that DSPF derivatives were colored.

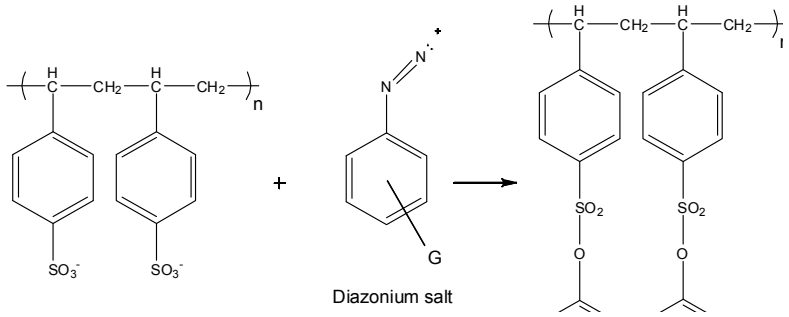

Scheme 1. Reaction scheme between polystyrene and diazonium salt with G as a substituent group.

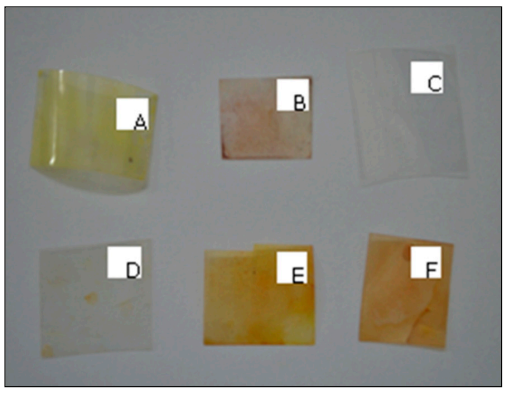

Figure 1. PS films modified with different aminocompounds: aniline (**A**); 3-aminophenol (**B**); 4-aminophenol (**C**); 2-chloroaniline (**D**); o-toluidine (**E**) y 4-nitroaniline (**F**).

As we can observe in Figure 2, the UV-vis spectra of PS and PSS films do not present any band in this region. The absorbance values of the spectra depend of the modification level; for this reason, the PSS modified with aniline and 3-aminophenol, and PSS modified with aniline present different absorbance values at similar wavelength. However, the wavelength of each band depends on the

conjugation level. Therefore, UV-vis spectral measurements provide evidence for the surface chemical modification of films. Thus, the PSS modified with aniline shows an excitation wavelength band at 375 nm; the PSS modified with aniline and 3-aminophenol presents a band at 375 nm; and the PSS modified with 3-aminophenol and 2-aminobenzylalcohol also presents a band at 480 nm. The excitation bands between 300 and 450 nm have been assigned to π–π^* transition in the azo groups. The band at 480 nm from the PSS modified with 3-aminophenol and 2-aminobenzyl alcohol could be due to the same transition red-shifted by conjugation with aromatic rings [56]. Moreover, Acevedo et al. demonstrated the modification of PS films using the same method [57]. Taking into account that Figure 1 clearly shows a visible change in the surface color in each PSS modified, the UV-vis spectroscopy presents the transition bands of the azo compound (Figure 2), and the published data by Acevedo et al., it is possible to ensure that the surface has been modified.

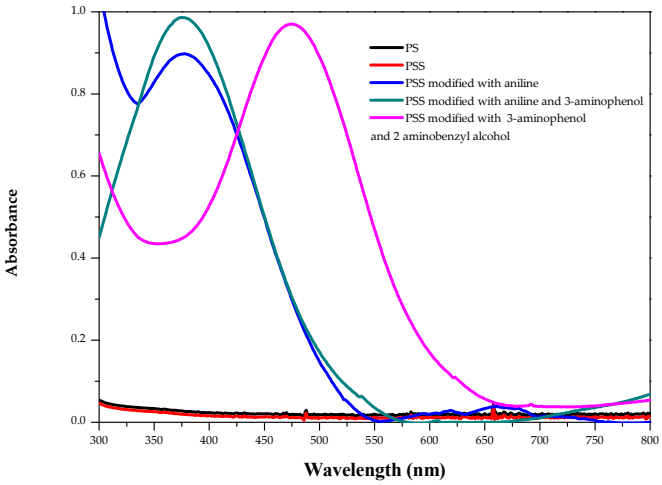

Figure 2. UV-visible spectra of unmodified and modified PS.

Deng et al. (2013) summarized the effect of 2D and 3D models of regularly arranged functional groups –COOH, –NH_2, –OH, –SO_3H, –CH_3, –SH and –PO_4H_2 on $CaCO_3$ crystallization [58]. In this context, DSPF functionalized with anionic moieties groups, for example, 3D arranged –SO_3H, should act as template with sites of nucleation active on its surface for obtaining selective CaOx crystals. Therefore, surface chemistry of modified polymer templates influences the nucleation and growth of selective crystal polymorphs, which are crucial in pathological mineralization, that is, HKS. Because of the different crystal forms of CaOx, different physicochemical properties are exhibited and they can behave very differently once inside the body, so reliable production of the required polymorph is crucial. The results of optical microscopy and scanning electron microscopy (SEM) analysis confirmed the presence of CaOx crystals deposited on DPSF with various aminocompounds. Most of these crystals exhibit the morphology and structure that is typically described for COM crystals, i.e., hexagonal shape; size 5.0 × 2.0 µm; faces {100} and {010} that are wide and exposed; defined edges, among others [59]. Similar CaOx crystals have been obtained using membrane lipid rafts [15], phospholipid monolayers [60–63] and SAMs [21] as crystallization templates. We analysed our results considering three aminocompouds: aniline, 2-trifluoromethyl aniline, and 4 nitro-aniline as substances carrying non-polar, polar and acid moieties, respectively. DSPF with non-polar chemical groups induced less CaOx crystals (Figure 3) and their size (±1.0–5.0 µm) was smaller than polar (Figure 4) and acidic DPSF (±5.0–10.0 µm), as shown by the images obtained by optical (see Figure S2) and SEM microscopy (see Figure S3). However, the quantity and shape of CaOx crystals obtained with DPSF with polar groups resulted more variable. For instance, agglomerated CaOx crystals were induced and crystallized on the surface (see Figure S3). We suspect that the surface chemical modification with aniline derivatives on organic film templates are responsible for topology surface modification,

which prompts a different scale of nucleation site points, resulting in chemical and physical aspects of the crystallization microenvironment that promote the active interaction between the functionalized film and inorganic mineral, producing a hybrid composite mineral.

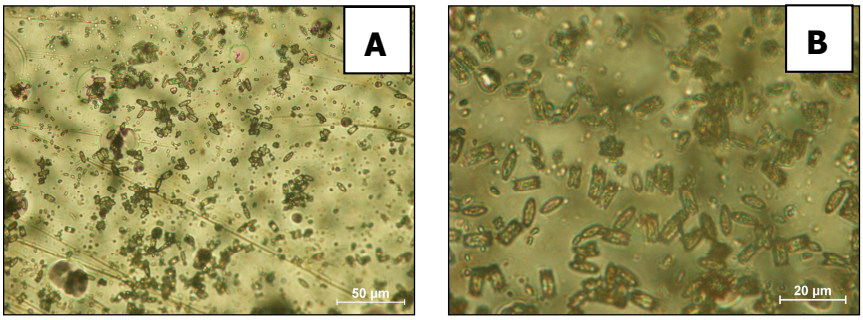

Figure 3. Optical image of CaOx crystals grown in polystyrene films sulphonated and diazotated with aniline. Low at 40× (**A**) and high at 100× (**B**) magnifications.

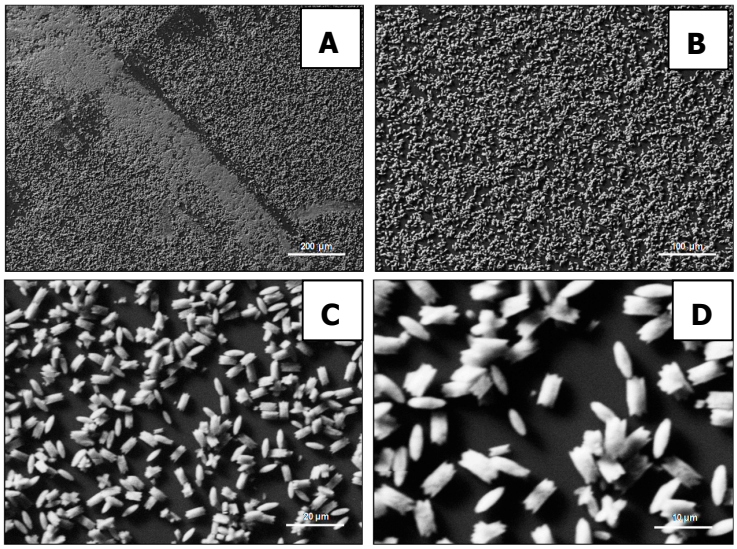

Figure 4. SEM images of CaOx crystals grown on PS films sulphonated and diazotated with 2-trifluoromethyl aniline. Low (**A**,**B**) and high (**C**,**D**) magnifications.

In order to determine the chemical composition of the different polystyrene films and CaOx crystals precipitated on PS surfaces, we used FTIR, and attenuated total reflectance (ATR) in conjunction with FTIR (ATR/FTIR), respectively. ATR/FTIR allows that samples, in liquid or solid matter state, be examined directly without further preparation. As the PS film presents a very thick chemical modification on the surface, it is very likely that the modified polymer spectra do not show bands that are attributable to the substituent groups (data not shown). This behavior could be due to the fact that the wavelength of maximum absorption depends on the presence of a particular amount of each chemical group, and its molar absorptivity. Taking into consideration that the polymers present huge quantities of the same chemical bonding group, the modification on the surface does not show an appreciable absorbance in comparison with the polymer backbone. In accordance with a previous work, molecules of water coordinated with molecules of calcium oxalate (H_2O • CaOx) produce a characteristic peak corresponding to mode bending at 1621 cm^{-1}, and stretch carboxylate metal (COO^- • M) appears at 1316 cm^{-1} [64]. FTIR spectra, as shown in Figure 5, show that the peak H_2O • CaOx (a) had a value of 1607 cm^{-1}, and the peak (COO^-) (b) has a value of 1313 cm^{-1}.

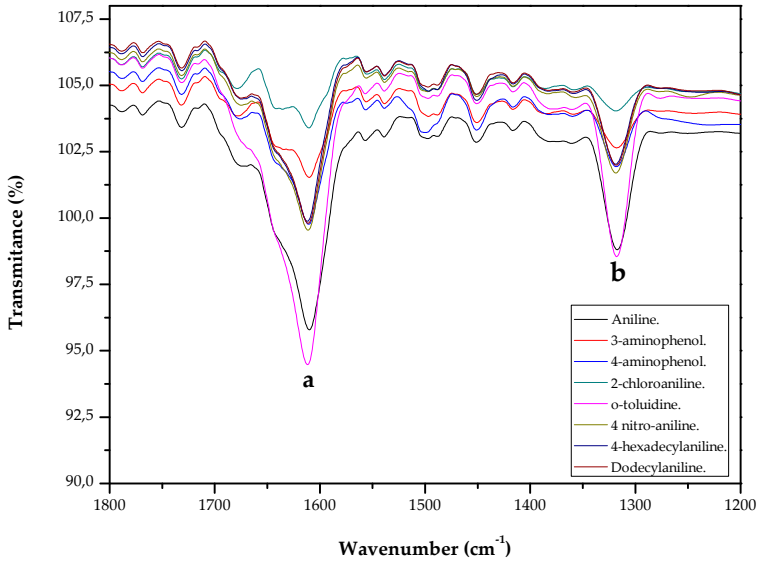

Figure 5. Fourier transform infrared spectroscopy (FTIR) spectra of CaOx crystals grown on sulphonated PS films, and diazotated with aniline, 3-aminophenol, 4-aminophenol, 2-chloroaniline, o-toluidine, 4-nitroaniline, 4-hexadecylaniline and dodecylaniline.

Because the inhibition of the CaOx nucleation is related to adsorption phenomena, the total amount of polymer adsorbed and the degree of surface coverage of the adsorbate on the inorganic crystal are important factors in determining the level of effectiveness of the polymer additive. In this context, energy-dispersive X-ray spectroscopy (EDS) measurements were performed on the surface of CaOx crystals; EDS analysis was used as a qualitative analysis, but spatially resolved to determine the elemental composition of calcium (Ca), carbon (C) and nitrogen (N) of DPSF and CaOx crystals deposited on their surface. The range of total Ca atomic weights, 21.06%, detected on the surface of COM crystals deposited on DPSF was in agreement with the theoretical value of pure CaOx [65–68]. In addition, an elemental mapping of the content of C (4S**B**) and N (4S**C**) showed a homogeneous distribution on PS films. Recently, we have performed an exhaustive SEM-EDS microanalysis of the elemental compositions of CaOx crystals grown under different experimental conditions by using electrocrystallization assays [43].

Complementing this study, a series of XRD measurement of CaOx grown on DSPF were also performed. XRD has advantages of reliability in qualitative analysis, and accuracy in quantitative analysis; being the choice test for the determination of crystal types in HKS [69,70]. In Figure 6, it is possible to observe diffraction peaks that are attributable to both COD as COM crystals. However, more intense peaks, detected at 2θ, such as 15°, 25°, 30° and 31°, correspond to crystal planes {1 0 1}, {2 1 1}, {2 0 2} and {0 2 0} of COM crystals respectively, which confirm what is observed by the above analysis [43,71–74]. In general, the use of this kind of functionalized DSPF film as a solid organic template could contribute to understanding the mechanisms underlying the formation of biologically important minerals, such as pathological urinary crystal forms, and it is kinetic on surface deposition. Moreover, an extra evaluation of the effect of the constituent ions' ratio, ionic strength, pH, presence of relevant inorganic ions, concentration and/or biological activity of macromolecules, supersaturation, and temperature found in urine, represents an advanced approach to test natural and/or synthetic additives with inhibiting and/or preventive properties of HKS formation. The current polymer surface approach is also important to the pharmaceutical industry.

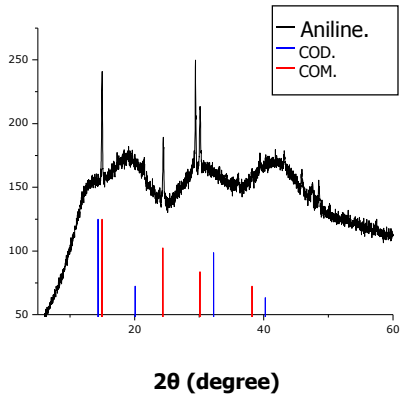

Figure 6. XRD patterns of the CaOx crystals grown on sulphonated PS films diazotated with aniline. The black line corresponds to the diazotated sulphonated polystyrene films sample pattern, and the red line to a standard pattern.

3. Materials and Methods

3.1. Reactants

Polystyrene of molecular weight 170.000 and 350.000 were purchased from Aldrich, and used as received. Trichloromethane anhydrous ($CHCl_3$) (Sigma-Aldrich, San Luis, MO, USA), sulfuric acid fuming ($H_2SO_4 \cdot (SO_3)x$) Sigma-Aldrich, sulfuric acid (H_2SO_4) 99,999% Sigma-Aldrich, hydrochloric acid (HCl) Sigma-Aldrich, sodium nitrate ($NaNO_2$) Sigma-Aldrich, sodium oxalate ($C_2Na_2O_4$) Sigma-Aldrich, calcium chloride dihydrate ($CaCl_2$) Merck, isopropilic acid (C_3H_8O) Sigma-Aldrich. All reagents were the highest grade commercially available.

3.2. Generation of Polystyrene Films

A 5% polymer solution in $CHCl_3$ was evaporated. An amount of 15 mL was selected as the volume of polymeric solution that was more appropriate for the formation of homogeneous films, and 36 h is enough for solvent evaporation. Using these conditions, it was possible to obtain reproducible films with optimal optical characteristics and approximately 150 μm of thickness.

3.3. Sulphonation of Polystyrene Films

The films were submerged in a 10% solution of fuming sulfuric acid (containing 65% of sulphur trioxide or SO_3) and 90% of concentrated sulfuric acid during 30 min. After that, films were washed with concentrated sulfuric acid in order to finalize the reaction and eliminate the sulphonating mix excess on the films, then rinsed with methanol, and finally with bidistilled water.

3.4. Diazotation of Sulphonated Polystyrene Films (DSPF)

An amount of 0.2 g of an aminocompound was added in a reaction recipient (RR). The aminocompound was dissolved in a water–alcohol solution (80:20 v/v) by sonication (10 min at high energy). A magnetic stirrer was put inside the recipient, and then the RR was put on a multi-stirrer containing a recipient with ice/water in order to keep the temperature below 5 °C. Different volumes of HCl and masses of $NaNO_2$ were simultaneously added in order to keep the molar ratio of aminocompounds:sodium nitrate:hydrochloric acid equal to 1:1:1, respectively. The following aminocompounds were utilized in the current work: aniline, 2-chloroaniline, 4-hexadecylaniline, 4-dodecylaniline, o-anisidine and 6-chloro-2,4-dinitroaniline.

3.5. Crystallization of CaOx

An amount of 3 mL of a $C_2Na_2O_4$ 1 mM solution was mixed with 3 mL of $CaCl_2$ 1 mM solution. The resultant solution was incubated in an oven, with regulable temperature for 24 h at 24 °C. Then, the DSPF were washed with deionized water, and dried at 24 °C for 6 h.

3.6. Optical, SEM-EDS, FTIR-ATR, UV-VIS and XRD Characterization of DSPF and CaOx Crystals

The UV-visible spectra of DPSF were performed by a HP 8452 spectrophotometer (Palo Alto, California, CA, USA). Fourier transform infrared spectroscopy (FTIR), and attenuated total reflectance in conjunction with FTIR (FTIR-ATR) analysis were performed by using a Bruker Tensor 27 spectrometer (Berlin, Germany) and Interspectrum Interspec p/n 200-X spectrometer (Toravere, Estonia), respectively. Optical images of CaOx crystals were obtained at a magnification 4×, 10×, 40× and 100×, exposure time of 20 ms to 2 s and a resolution of 2560 × 1920 pixels using a digital Nikon Eclipse E-600 camera (Shinagawa, Tokyo, Japan), connected to the microscope and computer. Image Pro-Plus, Media Cybernetics, USA, was used as morphometric software. For the analysis of samples at 100×, each film was put on a micro slide of 26 × 76 mm, thickness of 1 mm (pre-cleaned); a coverslip with immersion oil was put on the below preparation. Then, the lent microscope used for this purpose was cleaned with C_3H_8O. The morphology and polymorphism of CaOx crystals deposited on DPSF were studied by scanning electron microscopy (SEM) at a Carl Zeiss EVO MA10/Oxford at 20 kV. Elemental composition of DPSF and CaOx crystals was evaluated by using energy-dispersive X-ray spectroscopy (SEM-EDS) (Hitachi High-Tech Europe GmbH, Berlin, Germany). The DSPF are non-conductive samples, thus they were measured under a variable pressure mode and it was necessary to perform a metallic coating over them. The structure of CaOx crystals was evaluated by X-ray powder diffraction (XRD). XRD measurements were performed using a Siemens D-5000X X-ray diffractometer (Munich, Germany) with CuKθ radiation (graphite monochromator). The crystal structure was determined using CuKα radiation (40 kV); a 0.2° step, geometric scanning Bragg–Brentano (Π–Π) and the angle range from 5° to 70° (2θ) were performed. The Diffrac Plus was used as data control software.

4. Conclusions

We describe the preparation of different DPSF derivatives, and their influence as a polymeric template on the in vitro CaOx crystallization. DSPF was sulphonated by using a sulfuric acid solution. DPSF with different amino compounds were used to obtain polar, non-polar and acidic DSPF samples. This easy-way method for obtaining homogeneous DPSF as an organic template for the crystallization of CaOx provides an active functional group as the high negative charge onto an inert or commercial substrate, which should represent a key strategy to control the mineralization process in a similar way to biological molecules in the binding groups; that is, sulphonated polysacharide on the surface of inorganic-mineral-forming mineralized tissue which inhibits the growth and polymorphism of crystals. SEM observations revealed CaOx crystals deposited on DPSF surfaces. Moreover, measurements obtained from FTIR/ATR, SEM-EDS and XRD analysis confirmed the presence of COM crystals on DPSF. Natural and synthetic functionalized polymers with anionic groups influence the mineralization of inorganic compounds, which represents a great opportunity to obtain bio-inspired crystals with interesting features, sizes and morphologies.

Supplementary Materials: The following are available online at www.mdpi.com/2073-4352/7/3/70/s1. Figure S1: Chemical structures of amino-compounds used in the diazotation reaction of sulphonated polystyrene films. Figure S2: Optical images of CaOx crystals grown in polystyrene films sulphonated and diazotated. Figure S3: SEM images of CaOx crystals grown in polystyrene films sulphonated and diazotated. Figure S4: SEM-EDS of CaOx crystals grown on sulphonated polystyrene films diazotated with: 2-trifluoromethyl aniline (A) and aniline (B).

Acknowledgments: This research was supported by the Programme of International Scientific Cooperation (PCCI) PCCI12-038 CONICYT/MINCyT Call 2009 (Folio: 2009-112), FONDECYT 1140660 and FONDAP ACCDiS 15130011 granted by the Chilean Council for Science and technology (CONICYT), and partially funded by the Program URedes, Vice-presidency of Research and Development, University of Chile. P. Vásquez-Quitral thanks CONICYT fellowship.

Author Contributions: Patricio Vásquez-Quitral and Javier Toledo Arana conceived, designed and performed the experiments; Maria Cristina Miras, Diego Fernando Acevedo., and Cesar Alfredo Barbero contributed with reagents/materials/analysis tools; Andrónico Neira-Carrillo represents the senior author and he is principal investigator of the 1140660 FONDECYT'project and Program U-Redes, Vice-presidency of Research and Development, University of Chile, in which the current research work was done. Therefore, Andrónico Neira-Carrillo gives the first author the intellectual input, designs and approves the reported protocols of this study. Andrónico Neira-Carrillo has been responsible for the manuscript correction, proof reading during all paper submission, handling the revisions and re-submission process of the revised manuscript.

Conflicts of Interest: The authors declare no conflict of interest.

References

1. Aggarwal, K.P.; Narula, S.; Kakkar, M.; Tandon, C. Nephrolithiasis: Molecular mechanism of renal stone formation and the critical role played by modulators. *BioMed Res. Int.* **2013**, *2013*, 292953. [CrossRef] [PubMed]
2. Monje, P.; Baran, E. Characterization of calcium oxalates generated as biominerals in cacti. *Plant Physiol.* **2002**, *128*, 707–713. [CrossRef] [PubMed]
3. Neira-Carrillo, A.; Vásquez-Quitral, P. Formación de calculos renales de oxalato cálcico en mamíferos. *Av. Cienc. Vet.* **2010**, *25*. [CrossRef]
4. Rodgers, A.L.; Webber, D.; Ramsout, R.; Gohel, M.D. Herbal preparations affect the kinetic factors of calcium oxalate crystallization in synthetic urine: Implication for kidney stone therapy. *Urolithiasis* **2014**, *42*, 221–225. [CrossRef] [PubMed]
5. Holmes, R.P.; Assimos, D.G. Glyoxylate synthesis, and its modulation and influence on oxalate synthesis. *J. Urol.* **1998**, *160*, 1617–1624. [CrossRef]
6. Knight, J.; Jiang, J.; Assimos, D.G.; Holmes, R.P. Hydroxyproline ingestion and urinary oxalate and glycolate excretion. *Kidney Int.* **2006**, *70*, 1929–1934. [CrossRef] [PubMed]
7. Khan, S.R.; Canales, B.K. Genetic basis of renal celular dysfunction and the formation of kidney stones. *Urol. Res.* **2009**, *37*, 169–180. [CrossRef] [PubMed]
8. Marickar, Y.M.; Salim, A.; Vijay, A. Pattern of family history in stone patients. *Urol. Res.* **2009**, *37*, 331. [CrossRef] [PubMed]
9. Onaran, M.; Yilmaz, A.; Sen, I.; Ergun, M.A.; Camtosun, A.; Küpeli, B.; Menevse, S.; Bozkirli, I. Heparan sulfate gene polymorphism in calcium oxalate nephrolithiasis. *Urol. Res.* **2009**, *37*, 47. [CrossRef] [PubMed]
10. Brikowski, T.H.; Lotan, Y.; Pearle, M.S. Climate-related increase in the prevalence of urolitiasis in the United States. *Proc. Natl. Acad. Sci. USA* **2008**, *105*, 9841–9846. [CrossRef] [PubMed]
11. Basavaraj, D.R.; Biyani, C.S.; Browning, A.J.; Cartledge, J.J. The role of urinary kidney stone inhibitors and promoters in the pathogenesis of calcium containing renal stones. *EAU-EBU Update Ser.* **2007**, *5*, 126. [CrossRef]
12. Beiko, D.; Wollin, T. *The Consumer's Handbook of Urological Health*, 1st ed.; Canadian Urological Association: Quebec, QC, Canada, 2013; p. 267.
13. Wagner, C.A.; Mohebbi, N. Urinary pH and stone formation. *J. Nephrol.* **2010**, *23*, S165–S169. [PubMed]
14. El-Shall, H.; Jeon, J.H.; Abdel-Aal, E.A.; Khan, S.; Gower, L.; Rabinovich, Y. A study of primary nucleation of calcium oxalate monohydrate: II. Effect of urinary species. *Cryst. Res. Technol.* **2004**, *39*, 222–229. [CrossRef]
15. Campieri, C.; Campieri, M.; Bertuzzi, V.; Swennen, E.; Matteuzzi, D.; Stefoni, S.; Pirovano, F.; Centi, C.; Ulisse, S.; Famularo, G.; et al. Reduction of oxaluria after an oral course of lactic acid bacteria at high concentration. *Kidney Int.* **2001**, *60*, 1097–1105. [CrossRef] [PubMed]
16. Fasano, J.M.; Khan, S.R. Intratubular crystallization of calcium oxalate in the presence of membrane vesicles: An in vitro study. *Kidney Int.* **2001**, *59*, 169–178. [CrossRef] [PubMed]
17. Benitez, I.O.; Talham, D.R. Brewster angle microscopy of calcium oxalate monohydrate precipitation at phospholipid monolayer phase boundaries. *Langmuir* **2004**, *20*, 8287–8293. [CrossRef] [PubMed]

18. Benitez, I.O.; Talham, D.R. Calcium oxalate monohydrate precipitation at membrane lipid rafts. *J. Am. Chem. Soc.* **2005**, *127*, 2814–2815. [CrossRef] [PubMed]
19. Khan, S.R.; Maslamani, S.A.; Atmani, F.; Glenton, P.A.; Opalko, F.J.; Thamilselvan, S.; Hammett-Stabler, C. Membranes and their constituents as promoters of calcium oxalate crystal formation in human urine. *Calcif. Tissue Int.* **2000**, *66*, 90–96. [CrossRef] [PubMed]
20. Brown, C.M.; Novin, F.; Purich, D.L. Calcium oxalate crystal morphology: Influence of phospholipid micelles with compositions based on each leaflet of the erythrocyte membrane. *J. Cryst. Growth* **1994**, *135*, 523–532. [CrossRef]
21. Campbell, A.A.; Fryxell, G.E.; Graff, G.L.; Rieke, P.C.; Tarasevich, B.J. The nucleation and growth of calcium oxalate monohydrate on self-assembled monolayers (SAMS). *Scanning Microsc.* **1993**, *7*, 423–429. [PubMed]
22. Talham, D.R.; Backov, R.; Benítez, I.O.; Sharbaugh, D.M.; Whipps, S.; Khan, S.R. Role of lipids in urinary stones: Studies of calcium oxalate precipitation at phospholipid Langmuir monolayers. *Langmuir* **2006**, *22*, 2450–2456. [CrossRef] [PubMed]
23. Deng, S.P.; Ouyang, J.M. Effects of dipalmitoylphosphatidylcholine monolayers to the crystallization of calcium oxalate monohydrate from the solution containing chondroitin sulfate C. *Colloids Surf. A Physicochem. Eng. Asp.* **2005**, *257–258*, 47–50. [CrossRef]
24. Ouyang, J.-M. Chemical basis in the investigation of calcium oxalate stones. *Chem. Bull.* **2002**, *65*, 326.
25. Shirane, Y.; Kurokawa, Y.; Sumiyoshi, Y.; Kagawa, S. Morphological effects of glycosaminoglycans on calcium oxalate monohydrate crystals. *Scanning Microsc.* **1995**, *9*, 1081–1088. [PubMed]
26. Hess, B.; Meinhardt, U.; Zipperle, L.; Giovanoli, R.; Jaeger, P. Simultaneous measurements of calcium oxalate crystal nucleation and aggregation impact of various modifiers. *Urol. Res.* **1995**, *23*, 231–238. [CrossRef] [PubMed]
27. Ouyang, J.-M.; Deng, S.P. Controlled and uncontrolled crystallization of calcium oxalate monohydrate in the presence of citric acid. *J. Chem. Dalton Trans.* **2003**, *63*, 2486–2851. [CrossRef]
28. Tunik, L.; Fueredi-Milhofer, H.; Garti, N. Adsorption of sodium diisooctylsulfosuccinate onto calcium crystals. *Langmuir* **1998**, *14*, 3351–3355. [CrossRef]
29. Khan, S.R.; Whalen, P.O.; Glenton, P.A. Heterogeneous nucleation of calcium oxalate crystals in the presence of membrane vesicles. *J. Cryst. Growth* **1993**, *134*, 211–218. [CrossRef]
30. He, J.-Y.; Ouyang, J.-M. Circular patterns of calcium oxalate monohydrate induced by defective Langmuir-Blodgett film on quartz substrates. *Mater. Sci. Eng. C* **2009**, *29*, 288–291. [CrossRef]
31. Wiessner, J.H.; Hasegawa, A.T.; Hung, L.Y.; Mandel, G.S.; Mandel, N.S. Mechanisms of calcium oxalate crystals attachment to injured renal collecting duct cells. *Kidney Int.* **2001**, *59*, 637–644. [CrossRef] [PubMed]
32. De Koker, R.; McConnell, H.M. Circle to dogbone: Shapes and shape transitions of lipid monolayer domains. *J. Phys. Chem.* **1993**, *97*, 13419–13424. [CrossRef]
33. Kane, S.A.; Compton, M.; Wilder, N. Interactions determining the growth of chiral domains in phospholipid monolayers: Experimental results and comparison with theory. *Langmuir* **2000**, *16*, 8447–8455. [CrossRef]
34. Ouyang, J.-M.; Deng, S.-P. Formation of circular patterns of calcium oxalate crystals at defective sites of Langmuir–Blodgett films. *Colloids Surf. A* **2008**, *317*, 155. [CrossRef]
35. Loste, E.; Diaz-Marti, E.; Zarbakhsh, A.; Meldrum, F.C. Study of calcium carbonate precipitation under a series of fatty acid Langmuir monolayers using Brewster angle microscopy. *Langmuir* **2003**, *19*, 2830–2837. [CrossRef]
36. Cruz, A.; Vazquez, L.; Velez, M.; Perez-Gil, J. Influence of a fluorescent probe on the nanostructure of phospholipid membranes: Dipalmitoylphosphatidyl interfacial monolayers. *Langmuir* **2005**, *21*, 5349–5355. [CrossRef] [PubMed]
37. Ross, M.; Steinem, C.; Galla, H.-J.; Janshoff, A. Visualization of chemical and physical properties of calcium induced domains in DPCC/DPPS Langmuir-Blodgett layers. *Langmuir* **2001**, *17*, 2437–2447. [CrossRef]
38. Kang, Y.S.; Lee, D.K.; Lee, C.S.; Stroeve, P. In situ observation of domain structure in monolayers of arachidonic acid/γ-Fe_2O_3 nanoparticle complexes at the air/water interface. *J. Phys. Chem. B* **2002**, *106*, 9341–9346. [CrossRef]
39. An, Z.; Lee, S.; Oppenheimer, H.; Wesson, J.; Ward, M. Attachment of calcium oxalate monohydrate crystals on patterned surfaces of proteins and lipid bilayers. *J. Am. Chem. Soc.* **2010**, *132*, 13188–13190. [CrossRef] [PubMed]

40. Hug, S.; Grohe, B.; Jalkanen, J.; Chan, B.; Galarreta, B.; Vincent, K.; Lagugné-Labarthet, F.; Lajoie, G.; Goldberg, H.A.; Karttunena, M.; et al. Mechanism of inhibition of calcium oxalate crystal growth by an osteopontin phosphopeptide. *Soft Matter* **2012**, *8*, 1226. [CrossRef]
41. Sharma, V.; Park, K.; Srinivasarao, M. Colloidal dispersion of gold nanorods: Historical background, optical properties, seed-mediated synthesis, shape separation and self-assembly. *Mater. Sci. Eng. R.* **2009**, *65*, 1–38. [CrossRef]
42. Asselman, M.; Verkoelen, C.F. Crystal-cell interaction in the pathogenesis of kidney stone disease. *Curr. Opin. Urol.* **2002**, *12*, 271–276. [CrossRef] [PubMed]
43. Vargas Fernández, A. Efecto de Nanotubos de Carbono Como Moduladores de la Cristalización In Vitro de Oxalate Cálcico Mediante la Técnica de Electrocristalización. Ph.D. Thesis, Facultad de Ciencias Veterinarias y Pecuarias, Universidad de Chile, Santiago, Chile, 2016.
44. Fleming, D.E.; van Riessen, A.; Chauvet, M.C.; Grover, P.K.; Hunter, B.; van Bronswijk, W.; Ryall, R.L. Intracrystalline proteins and urolitiasis: A synchotron X-ray diffraction study of calcium oxalate monohydrate. *J. Bone Miner. Res.* **2003**, *18*, 1282. [CrossRef] [PubMed]
45. Kepa, K.; Coleman, R.; Grøndahl, L. In vitro mineralization of functional polymers. *Biosurf. Biotribol.* **2015**, *1*, 214–227. [CrossRef]
46. Leonor, I.B.; Kim, H.-M.; Balas, F.; Kawashita, M.; Reis, R.L.; Kokubo, T.; Nakamura, T. Formation of bone-like apatite on polymeric surfaces modified with $–SO_3H$ groups. *Mater. Sci. Forum* **2006**, *514–516*, 966–969. [CrossRef]
47. Leonor, I.B.; Kim, H.-M.; Balas, F.; Kawashita, M.; Reis, R.L.; Kokubo, T.; Nakamura, T. Functionalization of different polymers with sulfonic groups as a way to coat them with biomimetic apatite layer. *J. Mater. Sci. Mater. Med.* **2007**, *18*, 1923–1930. [CrossRef] [PubMed]
48. Leonor, I.B.; Kim, H.-M.; Balas, F.; Kawashita, M.; Reis, R.L.; Kokubo, T.; Nakamura, T. Surface charge of bioactive polyethylene modified with $–SO_3H$ groups and tts apatite inducing capability in simulated body fluid. *Key Eng. Mater.* **2005**, *284–286*, 453–456. [CrossRef]
49. Leonor, I.B.; Kim, H.-M.; Balas, F.; Kawashita, M.; Reis, R.L.; Kokubo, T.; Nakamura, T. Surface potential change in bioactive polymer during the process of biomimetic apatite formation in a simulated body fluid. *Mater. Chem.* **2007**, *17*, 4057–4063. [CrossRef]
50. Suzuki, S.; Whittaker, M.R.; Grøndahl, L.; Monteiro, M.J.; Wentrup-Byrne, E. Synthesis of soluble phosphate polymers by RAFT and their in vitro mineralization. *Biomacromolecules* **2006**, *7*, 3178–3187. [CrossRef] [PubMed]
51. Suzuki, S.; Rintoul, L.; Monteiro, M. J.; Wentrup-Byrne, E.; Grøndahl, L. In Vitro Mineralisation of Well-Defined Polymers and Surface. Ph.D. Thesis, Queensland University of Technology, Brisbane, Australia, 2007.
52. Stancu, I.C.; Filmon, R.; Cincu, C.; Marculescu, B.; Zaharia, C.; Tourmen, Y.; Basle, M.F.; Chappard, D. Synthesis of methacryloyloxyethyl phosphate copolymers and in vitro calcification capacity. *Biomaterials* **2004**, *25*, 205–213. [CrossRef]
53. Ethirajan, A.; Ziener, U.; Landfester, K. Surface-functionalized polymeric nanoparticles as templates for biomimetic mineralization of hydroxyapatite. *Chem. Mater.* **2009**, *21*, 2218–2225. [CrossRef]
54. Miyazaki, T.; Ohtsuki, C.; Akioka, Y.; Tanihara, M.; Nakao, J.; Sakaguchi, Y.; Konagaya, S. Apatite deposition on polyamide films containing carboxyl group in a biomimetic solution. *Mater. Sci. Mater. Med.* **2003**, *14*, 569–574. [CrossRef]
55. Kawai, T.; Ohtsuki, C.; Kamitakahara, M.; Miyazaki, T.; Tanihara, M.; Sakaguchi, Y.; Konagaya, S. Coating of an apatite layer on polyamide films containing sulfonic groups by a biomimetic process. *Biomaterials* **2004**, *25*, 4529–4534. [CrossRef] [PubMed]
56. Sıdıra, Y.G.; Sıdıra, İ.; Taşalb, E.; Ermişc, E. Studies on the electronic absorption spectra of some monoazo derivatives. *Spectrochim. Acta A Mol. Biomol. Spectrosc.* **2011**, *78*, 640–647. [CrossRef] [PubMed]
57. Brogli, M.F.; Suarez, S.; Soldera, F.; Mücklich, F.; Barbero, C.A.; Bellingeri, R.; Alustiza, F.; Acevedo, A. Direct laser interference patterning of polystyrene films doped with azo dyes, using 355 nm laser light. *Appl. Surf. Sci.* **2014**, *300*, 86–90. [CrossRef]
58. Deng, H.; Shen, X.C.; Wang, X.M.; Du, C. Calcium carbonate crystallization controlled by functional groups: A mini-review. *Front. Mater. Sci.* **2013**, *7*, 62–68. [CrossRef]
59. Borissova, A.; Goltz, G.; Kavanagh, J.; Wilkins, T. Reverse engineering the kidney: Modelling calcium oxalate monohydrate crystallization in the nephron. *Med. Biol. Eng. Comput.* **2010**, *48*, 649–659. [CrossRef] [PubMed]

60. Whipss, S.; Khan, S.R.; O'Palko, F.J.; Backov, R.; Talham, D.R. Growth of calcium oxalate monohydrate at phospholipid Langmuir monolayers. *J. Cryst. Growth* **1998**, *192*, 243–249. [CrossRef]
61. Letellier, S.R.; Lochhead, M.J.; Campbell, A.A.; Vogel, V. Oriented growth of calcium oxalate monohydrate crystals beneath phospholipid monolayers. *Biochim. Biophys. Acta* **1998**, *1380*, 31–45. [CrossRef]
62. Ouyang, J.M.; Deng, S.P.; Zhong, J.P.; Tieke, B.; Yu, S.Y. Crystallization of calcium oxalate monohydrate at dipalmitophosphatidylcholine monolayers in the presence of chondroitin sulfate A. *J. Cryst. Growth* **2004**, *270*, 646–654. [CrossRef]
63. Deng, S.P.; Ouyang, J.M.; Xie, Y.S.; Xing, F.Y. Circular patterns of calcium oxalate crystals induced by defective Langmuir-Blodgett films. *Sci. China Ser. B Chem.* **2008**, *51*, 25–30. [CrossRef]
64. El-Shall, H.; Jeon, J.-H.; Abdel-Aal, E.A.; Khan, S.; Gower, L.; Rabinovich, Y. A study of primary nucleation of calcium oxalate monohydrate: I. Effect of supersaturation. *Cryst. Res. Technol.* **2004**, *39*, 214. [CrossRef]
65. Didenko, L.; Tolardava, E.; Perpanova, T.; Shevlyagina, T.; Boravaya, Y.; Romanova, Y.; Cazzaniga, M.; Curia, R.; Milani, R.; Savoia, C.; et al. Electron microscopy investigation of urine stones suggests how to prevent post-operation septic complications in nephrolithiasis. *J. Appl. Med. Sci.* **2014**, *3*, 2241–2328.
66. Kumar, N.; Singh, P.; Kumar, S. Physical, X-ray diffraction and SEM studies of uroliths. *Indian J. Biochem. Biophys.* **2006**, *43*, 226–332. [PubMed]
67. Abdel-Aal, E.; Daosukho, S.; El-Shall, H. Effect of supersaturation ratio and Khella extract on nucleation and morphology of kidney stones. *J. Cryst. Growth* **2009**, *311*, 2673–2681. [CrossRef]
68. Neira-Carrillo, A.; Luengo-Ponce, F.; Vásquez-Quitral, P.; Yazdani-Pedram, M.; Fernández, M.S.; Cölfen, H.; Arias, J.L. Sulfonated polymethylsiloxane as an additive for selective calcium oxalate crystallization. *Eur. J. Inorg. Chem.* **2015**, *7*, 1167. [CrossRef]
69. Ghosh, S.; Basu, S.; Chakraborty, S.; Mukherjee, A.K. Structural and microstructural characterization of human kidney stones from eastern India using IR spectroscopy, scanning electron microscopy, thermal study and X-ray Rietveld analysis. *J. Appl. Cryst.* **2009**, *42*, 629–635. [CrossRef]
70. Giannossi, M.L.; Summa, V. New mixed urinary stone: Review of classification scheme. *Urologist* **2012**, *1*, 2.
71. Zhang, D.; Qi, L.; Ma, J.; Cheng, H. Morphological control of calcium oxalate dehydrate by a double-hydrophilic block copolymer. *Chem. Mater.* **2002**, *14*, 2450–2457. [CrossRef]
72. Laffite, G.; Leroy, C.; Bonhomme, C.; Bonhomme-Coury, L.; Letavernier, E.; Daudon, M.; Frochot, V.; Haymann, J.P.; Rouzière, S.; Lucas, I.T.; et al. Calcium oxalate precipitation by diffusion using laminar microfluidics: Toward a biomimetic model of pathological microcalcifications. *Lab Chip* **2016**, *16*, 1157. [CrossRef] [PubMed]
73. Kirboğa, S.; Öner, M. Inhibition of calcium oxalate crystallization by graft copolymers. *Cryst. Growth Des.* **2009**, *9*, 2159–2167. [CrossRef]
74. Neira-Carrillo, A.; Vásquez-Quitral, P.; Sánchez, M.; Vargas-Fernández, A.; Silva, J.F. Control of calcium oxalate morphology through electrocristallization as an electrochemical approach for preventing pathological disease. *Ionics* **2015**, *21*, 3141–3149. [CrossRef]